Valence Ionization of Water Clusters: From Isolated Molecules to Bulk

Silko Barth,[†] Milan Ončák,[‡] Volker Ulrich,[†] Melanie Mucke,[†] Toralf Lischke,[†] Petr Slavíček,*[,‡] and Uwe Hergenhahn*[,†,¶]

Max-Planck-Institut für Plasmaphysik, EURATOM Association, Boltzmannstrasse 2, 85748 Garching, Germany, and Department of Physical Chemistry, Institute of Chemical Technology, Prague, Technicka 5, Prague 6, 166 28, Czech Republic

Received: June 30, 2009; Revised Manuscript Received: September 22, 2009

The valence photoelectron spectra of water clusters are studied experimentally and by ab initio calculations. The size dependence of the vertical ionization energy of the outermost orbitals is explicitly shown. A shift toward lower values is observed. For small cluster sizes, it can be rationalized as an effect of charge delocalization as the system is becoming more extended. Ionization energies of larger clusters decrease linearly with inverse cluster radius and asymptotically approach the value of liquid water. In the calculations, we apply a reflection principle approach based on sampling a quantum mechanical distribution of different initial-state geometries to clusters. An excellent agreement of peak shapes calculated thus with measured ones is shown. Using additional polarization fields, the extension of this approach to the photoionization of liquid water is demonstrated. Upon deuteration of the water clusters, we experimentally and theoretically find slightly larger absolute values of the vertical ionization energies. We suggest that the measurement of electron ionization energies can be used as an alternative means to characterize water cluster sizes, which can complement the use of scaling laws.

Introduction

The binding energies of the valence electrons in an isolated water molecule are well-known.[1] In an assembly of water molecules, that is, liquid water, these binding energies change due to the formation of a hydrogen bridge network between the single molecules. A direct experimental investigation of these changes by photoelectron spectroscopy has only been possible recently.[2] A detailed explanation of the observations remained open however since, besides changes in initial-state orbital energy, other factors may influence the observed binding energies. These are (1) polarization screening of the positive charge in the final state and (2) work function effects due to surface charges. To delineate the contributions of these mechanisms is of great interest as it may yield further insights into the phenomena of hydrogen bonding and solvation of a positive charge by water molecules.

In this work, we have investigated the valence photoelectron spectrum of small, free water clusters. We present a full spectrum of the valence orbitals with high energy resolution, and we discuss the position of the highest occupied molecular orbital (HOMO) photoelectron peak in dependence of cluster size. We demonstrate that our values extrapolate linearly toward the limiting value for liquid water when plotted as a function of inverse cluster size. To gain further insight into the nature of interactions in the water clusters, we have modeled a range of photoelectron spectra by ab initio quantum chemical calculations.

Photoelectron spectra of water clusters were presented earlier, but to the best of our knowledge, no systematic studies of their dependence on cluster size have been carried out. The outer valence spectrum of the water dimer was studied with a gas discharge source.[3] Björneholm et al.[4] used synchrotron radiation for excitation and greatly extended the energy range of this early work. They reported the outer-valence- and the core-level (XPS) photoelectron spectra, the latter already for a number of cluster sizes. A valence photoelectron spectrum with improved apparatus resolution was published by Öhrwall et al.[5] In both studies, only an estimate of the cluster size as "large" was given. In a number of experiments, the ionic species produced by cluster photoionization were recorded. The appearance energy for the water dimer cation $(H_2O)_2^+$ was measured as 11.21(9) eV.[6] Larger water clusters subsequent to ionization tend to relax by emission of at least one neutral OH group, such that only protonated species of the type $(H_2O)_nH^+$ [7,8] are observed in a mass spectrum. This shows that clusters are left with a substantial amount of internal energy by the photoionization process, which can be explained from the large difference between neutral and ionic cluster geometries. The adiabatic ionization energy of the respective water cluster species can therefore not be determined by a vertical ionization process, such as single-photon photoionization. For the water dimer cation, an adiabatic value of 10.8−10.9 eV is found from a charge exchange reaction,[9] which is significantly lower than the photoionization result given above. Comparison of appearance energies measured with seeded cluster beams[7] should take into account that release of inner energy of the cluster cations can take place by neutral monomer evaporation of seeding gas atoms.[10] A systematic study of the size-resolved appearance energies of $(H_2O)_nH^+$ cluster fragments appeared recently[11] and will be discussed below.

The experimental results presented in this paper are supplemented by theoretical data. We calculate the equilibrium geometries and the vertical ionization potentials of water clusters with 2−8 molecules. The contribution of nuclear effects to the

* To whom correspondence should be addressed. E-mail: Petr.Slavicek@vscht.cz (P.S.); uwe.hergenhahn@ipp.mpg.de (U.H.).
† Max-Planck-Institut für Plasmaphysik.
‡ Institute of Chemical Technology, Prague.
¶ Address: IPP, c/o Helmholtz-Zentrum Berlin, Albert-Einstein-Str. 15, 12489 Berlin, Germany.

10.1021/jp906113e CCC: $40.75
Published on Web 10/26/2009

width of the valence peaks is modeled by the use of the reflection principle. We test different ab initio approaches, showing their mutual consistency for describing ionization of small clusters. The shift in the position of photoelectron peaks is driven by two phenomena, charge delocalization and electronic polarization. The former effect dominates for small clusters, while the latter is important to reach the bulk limit. We have therefore also applied a dual approach, in which small water clusters are immersed in a polarizable dielectric continuum.

Ionization spectra have already been studied theoretically for one water molecule[12] and for simplified models of liquid water[13−15] as well as ice.[16] The importance of thermal and electronic broadening in the liquid water ionization spectra has been investigated, and their contributions were found to be of comparable magnitude.[13]

So far, properties of small cationic water clusters were studied mostly in the local minima conformations, for example, vertical ionization energies were calculated,[17] and the structure of the ionized clusters, in particular of a water dimer cation,[18,19] was investigated. Ab initio dynamics studies of $(H_2O)_n^+$ clusters up to $n = 6$ have been carried out in order to address induced structural changes in the ionized-state dynamics.[20−25] To the best of the authors' knowledge, calculations in this paper represent the first attempt to model both the position and shape of the ionization spectra of small water clusters in the gas phase. Cabral do Couto et al. have calculated orbital energies for water clusters of several sizes.[14] However, their cluster structures where taken as samples from a molecular dynamics simulation of liquid water with an effective interaction potential (TIP5P) and might therefore differ from the clusters with optimized structure which are covered here. Size dependence in that work was considered to prove convergence to the bulk limit.

Methods Section

Experimental Section. Free water clusters were produced by supersonic expansion of water vapor through a conical nozzle. Water was kept in a heated reservoir inside of an expansion chamber. Details of a similar setup have been published.[26] Our design uses a total reservoir volume of about 20 mL, which allows for about 6 h of uninterrupted operation.[27] The water vapor expands into the vacuum via a conical copper nozzle. The nozzle is mounted on a 4-VCR nut (Cajon, Solon, OH), which is heated separately from the reservoir to avoid condensation. For the measurements shown here, a nozzle diameter of 80 μm, a half opening angle of 15°, and a length of 1100 μm were used. Temperatures of the reservoir and the nozzle are measured by thermocouples. Seeding of cluster production by coexpansion with an inert gas is possible but was not employed here. Cluster sizes were determined from the expansion parameters by a scaling law as derived from mass spectroscopy by Bobbert et al.[28] The overall error of cluster sizes is estimated as 35%. A detailed discussion of expansion parameters and cluster sizes determined is given in the Supporting Information. Further details of our setup can be found in ref 27.

A conical skimmer separated the expansion chamber from the main chamber, in which the interaction with synchrotron radiation from the storage ring BESSY II (Berlin, Germany) takes place. Electrons from photoionization and subsequent reactions of the clusters are collected by a commercial hemispherical spectrometer (Scienta ES 200). The water reservoir and expansion nozzle can be adjusted relative to the skimmer with an *xyz*-manipulator. The spectrometer is mounted under the magic angle of 54.7° with respect to the horizontal and within a plane perpendicular to the photon propagation direction. Details about this part of the apparatus have been published.[29] For the water cluster experiments, other than that in ref 29, the main chamber was pumped by a cryopump of 900 L/s nominal speed (Leybold RPK 900), into which the cluster jet was directed. Additionally, a 360 L/s turbo pump was used. Under these conditions, the expansion chamber pressure was in the $10^{-4}-10^{-3}$ mbar range, and the main chamber pressure around 10^{-6} mbar.

Photons were provided by the UE 112 lowE PGMa beamline.[30] The undulator was set to produce horizontally linearly polarized radiation. The 600 lines/mm plane grating was used in grazing incidence. The pass energy and entrance slit of the hemispherical electron analyzer were set to 20 eV and 500 μm, respectively. The apparatus broadening of the spectra thus was dominated by the analyzer contribution and is estimated to be approximately 50−80 meV, in good agreement with the width of the adiabatic photoelectron peak of the monomer $1b_1$ orbital (HOMO). Photon energies were used without correction (error estimated less than ±0.1 eV), and spectrometer energies were corrected to yield a binding energy for the monomer $1b_1$ adiabatic peak of 12.615 eV.[1]

Spectra recorded at a 30 eV photon energy were corrected for the energy dependence of the electron spectrometer transmission. This was estimated by measuring the area of the He 1s line, normalized to the flux of a GaAs photodiode, for different kinetic energies. This procedure may, in principle, suffer from the influence of higher-order radiaton on the photodiode current. Relative areas of the monomer $3a_1$ and $1b_2$ photolines, however, after normalization were within the span of earlier literature values (see below).[31,32] For the spectrum recorded at 60 eV, no transmission correction was performed.

The condensation degree of our cluster jet, defined as the cluster signal versus the total signal, under typical expansion conditions is 15−75%. To isolate the cluster contribution, we have therefore subtracted a reference spectrum of the water monomer contribution. In principle, such spectra can be obtained by operating the source at low temperatures. However, we found that in our setup, the cluster signal is negligible if the source is fully retracted from the skimmer and moved away from the axis connecting the skimmer opening and interaction region. As the intensity ratio between the cluster + monomer and the reference spectrum is not a priori known, the latter was scaled such that the well-resolved vibrational structure of the $1b_1$ and $3a_1$ lines was removed by the subtraction. To accomplish this, a minor, reproducible energy adjustment of the reference spectrum was necessary, which amounted to 7.5−30 meV, well within the apparatus resolution. We assume an experimental origin of these energy differences, which could either be buildup of charged species in the interaction region or slightly differing positions of the supersonic jet for clusters as compared to those for monomer species.

A separate series of data (not shown) was recorded to compare the spectra of water clusters with those of heavy water (D_2O). Analyzer and beamline settings were set as before. The expansion conditions were made as similar as possible (see Supporting Information for details), and the photon energy was varied between 27 and 41 eV in 2 eV steps for both isotopes. Results discussed below are from an average over all spectra for the respective isotope.

Another separate experiment was used to derive relative intensities for the monomer and cluster outer valence lines at $h\nu = 61$ eV. There, water clusters were produced by expanding water vapor from a heated, external reservoir through a copper

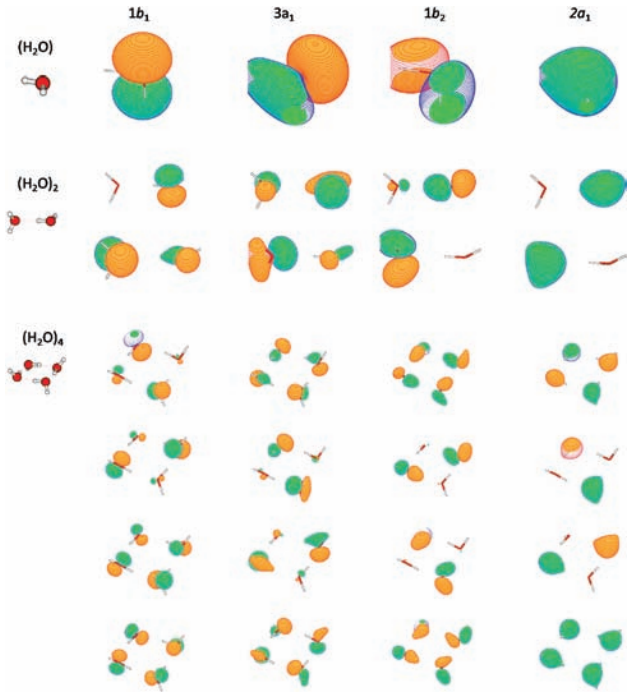

Figure 1. Molecular orbitals of the water monomer, dimer, and tetramer, calculated at the MP2/aug-cc-pVDZ level.

nozzle as described in ref 29. The nozzle was at room temperature, and seeding with Ne gas was used to foster condensation. Due to the use of a seeding gas, scaling laws as discussed above cannot be used to determine the cluster size in this case. We have therefore used the HOMO ionization energy found in this experiment together with the size−ionization energy relation proposed in this work to estimate a cluster size (see below).

Peak positions from the experimental spectra were extracted either as the peak maxima or by a least-squares fit of a sum of Gaussian profiles plus a linear background to the experimental data. Only the part of the spectra containing the $1b_1$ peak was subjected to this analysis. The background due to overlap with the $3a_1$ cluster peak was represented by another Gaussian of fixed width and position.

Calculation of Photoelectron Spectra. Photoionization spectra were calculated at ab initio level for various small water clusters $(H_2O)_n$, $n = 1-6$, 8. Small water clusters up to $n = 5$ are represented by cyclic structures; for $(H_2O)_6$, both prism and cage structures were calculated, and the $(H_2O)_8$ cluster was considered in a cubic geometry. Ground-state geometries were calculated at the MP2 level.

We have calculated both the position of the photoelectron peaks and the shape of the photoelectron spectra for the respective clusters. The spectra included the first $3n$ ionized states, that is, all outer valence ionization bands were included in the calculations. For illustration, the shapes of the respective orbitals from our calculations are shown in Figure 1. (Note that quasi-degenerate orbitals for polymeric systems are not unique and may be easily transformed to different shapes by various approaches.)

Several different ab initio approaches were employed to model the spectra.

(a) PMP2/TDDFT approach. Here, the first ionization potential is calculated using the unrestricted MP2 method, with a subsequent annihilation of the higher spin components (PMP2).[33] Energies corresponding to the ionization from (HOMO-i) orbitals are then calculated by adding the appropriate excitation energy of the ionic state to the first ionization potential. We have used the BHandHLYP functional for the TDDFT calculation. Comparison with higher-level electronic structure methods shows that the PMP2 method in a combination with the TDDFT/BHandHLYP excitation energies provides an accurate estimate of ionization potentials.[34]

(b) CASPT2 method. Ionization potentials are calculated at the CASPT2 level. In this case, $3n$ states are state-averaged in the CASSCF wave function of the ion, with an active space composed of $(6n - 1)$ electrons in $3n$ orbitals. This choice guarantees that excitations of all $1b_1$, $3a_1$, and $1b_2$ electrons of each water molecule into a singly occupied molecular orbital (SOMO) are included. Dynamical correlation is then added via a state-specific CASPT2 procedure. A level shift of 0.4 hartree is applied throughout. Unlike in the previous method, all ionized states are calculated at the same level.

(c) EOM-IP approach.[35] In this method, the ionization potentials are calculated directly by the EOM-IP-CCSD method, with excitations described as promotion of electrons from the highest occupied $3n - 1$ orbitals into the SOMO orbital.

We later show that the three approaches yield rather similar results. In order to model ionization within bulk water, we have therefore chosen the computationally efficient PMP2/TDDFT approach for small water clusters combined with a dielectric continuum description of the surrounding water medium (the polarizable continuum model, PCM). Since photoionization is a vertical process, the concept of nonequilibrium solvation has to be used; only the optical component of the solvent response has to be included in the calculation.[36,37] The reliability of the PMP2/TDDFT/NonEqPCM approach for a description of ionization in aqueous solutions was tested recently.[37]

Density functional methods are known to suffer from the problem of an artificial charge delocalization.[38] We have therefore compared the charge distributions calculated at the DFT level with those calculated at the single-state CASPT2 level. In both cases, charges were calculated using the Mulliken scheme. We found that the DFT approach provides an essentially identical picture of the charge delocalization in water clusters as the CASPT2 method. For the water trimer $(H_2O)_3$ as the case study, the delocalization of the charge at the CASPT2/aug-cc-pVDZ level is calculated to be 31, 40, and 35% for the $1b_1$, $3a_1$, and $1b_2$ bands, respectively (100 random geometries from a Wigner distribution, averaged over all transitions of each band). At the TDDFT/BH-LYP/aug-cc-pVDZ level, these values are slightly increased to 32, 46, and 42%.

In order to calculate the shapes of the photoionization spectra at the ab initio level, we have applied several approximations.

(1) The reflection principle[39] was used. In this approach, the ground state density $|\Psi_i|^2$ is projected onto the ionized-state curve and further to the energy axis (see Figure 2). Solvated water upon the ionization rapidly leaves the Franck−Condon region, and good performance of the method can therefore be expected. In this approach, the ionization energy at a given geometry is determined as the difference between the ionized-state energy in the respective geometry and the ground-state energy at its local minimum. The zero-point energy is fully included in the ground state, while only half of it is accounted for in the ionized state (representing the kinetic energy of the excited state). For the calculation of the local minima energies, the MP2 energy has been used for the CASPT2 calculations and the CCSD energy in the EOM-IP model.

(2) The photoionization cross section is considered to be independent of the geometry and of the orbital from which we

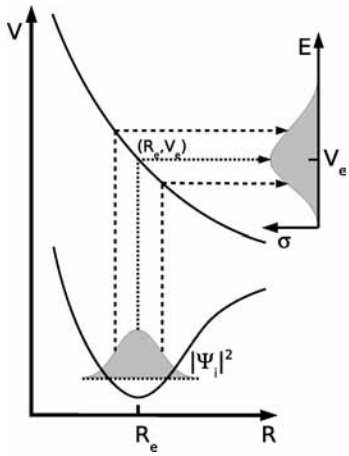

Figure 2. Sketch of the reflection principle, which was used to estimate nuclear effects on the positions of spectral lines (see text for details). A molecule in its ground state (lower potential curve, solid line) is excited by a vertical ionization process (that is, photoionization, electron impact ionization). The upper configuration has a dissociative potential curve (upper solid line) at the ground-state geometry. The probability density $|\Psi_i|^2$ of the ground-state wave function (lower, horizontal gray shaded region) is thus mapped onto an energy distribution in the ionization spectrum (vertical, gray shaded region). V and E designate potential energy and photoionization energy axes, respectively, with V_e as the value at the equilibrium configuration R_e; σ designates the photoionization cross section. For simplicity, only one nuclear coordinate is drawn. The application to ionized states with a bound potential is analogous.

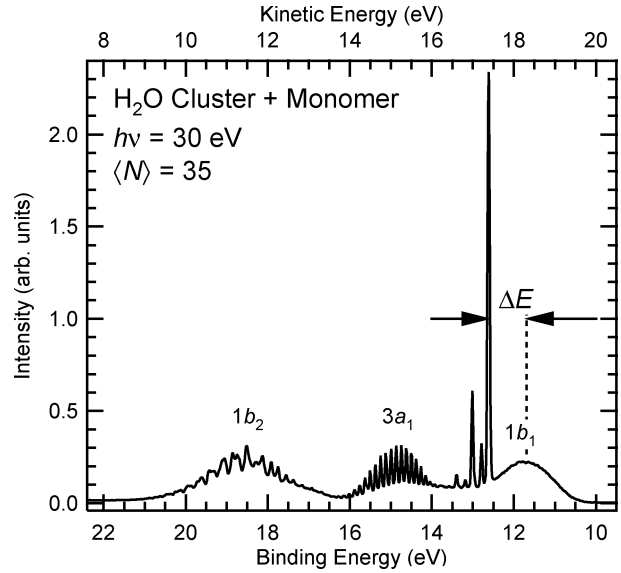

Figure 3. Outer valence photoelectron spectrum of a mixture of water clusters and uncondensed water molecules. Sharp lines result from the vibrational structure of the monomers.[1] Features are assigned to ionization of the three outer valence orbitals of water as designated in the figure. The shift of the cluster HOMO peak to the adiabatic line of the monomer, ΔE, is discussed below.

ionize. The former assumption will affect the shape of the peaks, while the latter will influence the relative intensities of different bands. The second approximation can be rather crude; however, we suggest it might be reasonable for modeling photoionization spectra obtained with high photon energies. Below, we will further comment on the quality of this approximation by comparing the results to experimental values of the cross section.

(3) Due to the previous two approximations, the shape of the spectrum is defined solely by the ground-state density. There are two effects potentially playing a role, thermal broadening of the spectra and broadening due to the quantum delocalization. Ideally, both effects would be covered by using, for example, path integral techniques.[40] Here, we have identified the quantum broadening to be the dominant contribution to the spectral broadening and further omitted the thermal effects (see Supporting Information for details).

Quantum delocalization was described within the harmonic approximation with frequencies calculated at the MP2 level. The low-frequency anharmonic modes below 500 cm^{-1} (62 meV) were completely neglected. To calculate the spectra via the reflection principle, evaluation of a multidimensional integral over the ground-state density is required. This has been done via a Monte Carlo procedure, that is, points from the multidimensional integral were chosen based on their probability in the Wigner function and subsequently summed with the same weight. One thousand sample points were used for $(H_2O)_n$, $n = 1-4$ and 600 sample points for the larger clusters with $n = 5, 6, 8$ (400 points in case of the EOM-IP approach).

The ionization potentials for water clusters are not critically dependent on the choice of the basis set. We have therefore used a modest choice, the 6-31++g** basis. This allows us to evaluate photoelectron spectra, including their widths, which are converged with respect to the Monte Carlo sampling procedure. A certain quantitative disagreement with the experiment is however necessarily expected. For the vertical ionization potentials of the water monomer, calculated at the CASPT2/6-31++g** level, the values of 12.42, 14.69, and 18.94 eV are found for electrons in $1b_1$, $3a_1$, and $1b_2$ orbitals. This differs from our experiment, with 12.72(2), 14.92(2), and 18.86(2) eV, by some tenth of an eV. The origin of these differences may be attributed partially to the quality of the employed basis set. With a somewhat larger aug-cc-pVDZ basis, the calculated ionization energies of 12.57, 14.88, and 18.99 eV are in much better agreement for both the $1b_1$ and $3a_1$ transitions, while the $1b_2$ energy is still overestimated. Overall, as these deviations are below 3%, the 6-31++g** basis set is used as a compromise between the accuracy and feasibility of the calculations. For the water dimer, the first six ionization energies for a 6-31++g** basis set are underestimated on average by 0.15 eV with respect to the aug-cc-pVDZ values.

The following quantum chemical program packages were used for the calculations: Gaussian (TDDFT, MP2, PCM),[41] Molpro (MP2, CASPT2),[42] ACES2 (EOMIP-CCSD),[43] and Turbomole (charges in TDDFT).[44]

Results

Here, we will first discuss the experimental and calculated results for the gross spectral shape. In a second subsection, we will treat the size dependence of the ionization energies in detail.

Shape of the Photoelectron Spectrum of Water Clusters. A representative experimental photoelectron spectrum of a mixture of water monomers and clusters is shown in Figure 3. Spectra consist of a series of sharp lines, which represent the vibrational progression of outer valence photoionization from monomers superimposed to smooth, structureless features which we attribute to cluster photoemission. The photoelectron spectrum of water monomers is well-known.[1,45] Ionization of the HOMO of $1b_1$ symmetry (see Figure 1) is hardly of any influence on the molecular bonding and thus results mainly in transitions to the molecular ionic vibrational ground state ($v' = 0$), the adiabatic peak. Ionization of the $3a_1$ orbitals results in a cation of linear equilibrium geometry and thus in strong bending excitations, and ionization of the $1b_2$ orbital leads to a

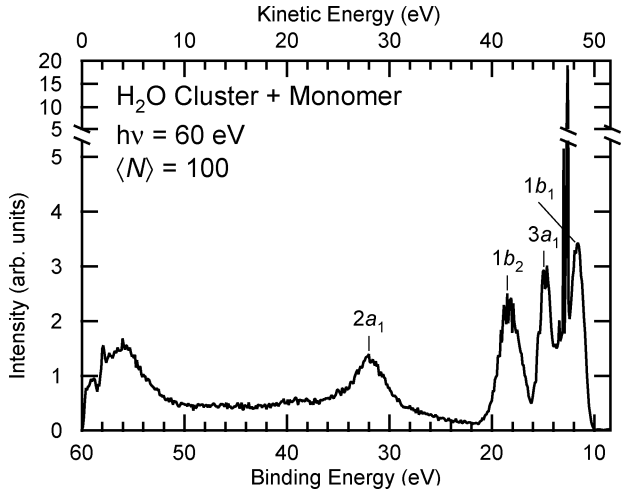

Figure 4. Complete valence photoelectron spectrum of a mixture of water clusters and uncondensed water molecules.

rather complicated final-state dynamics.[45,46] In our spectra, we avoided the use of a seeding gas and, possibly because of that, encountered a somewhat larger contribution of monomer photoemission than in earlier work.[4,5]

The full valence band photoelectron spectrum of water clusters with $\langle N \rangle = 100$ is shown in Figure 4. Additionally to the outer valence structure discussed below, the spectrum shows the water inner valence orbital ($2a_1$) at a binding energy of 32.0 eV, in between the gas-phase reference value of 32.6 eV[2,31] and the orbital energy in the liquid of 30.9(1) eV.[2] The photoelectron line from this state is broad already in the gas phase. This might be due to an admixture of satellite (2h−1p) states in this binding energy region, as discussed in ref 46.

It is interesting to compare our experimental spectra to our calculations. In order to do so, for $h\nu = 30$ eV (Figure 3), a reference spectrum recorded with an uncondensed beam was subtracted to yield the cluster photoelectron spectrum in Figure 5, bottom panel (see Experimental Section for details). After subtraction of the monomer contribution, all fine structure in the spectrum is gone, although our apparatus resolution would certainly suffice to resolve more details. This is attributed to the multitude of electronic and vibrational states in clusters, which smears out finer details of the structure. The $3a_1$ band is broadened to a larger extent than the remaining two orbitals as the former undergoes a splitting due to its participation in the hydrogen bonding between the clusters (see below). Contrary to the situation in the gas phase, photoemission from this band overlaps with features of the $1b_1$ orbital, which participates to some extent in hydrogen bonding of larger structures. The remaining weak structure on the $1b_2$ cluster line may result from imperfections in the scaling of the subtracted monomer spectrum.

Qualitatively, the comparison of our calculated peak shapes to both our experimental cluster spectrum as well as the literature spectrum of liquid water is fully satisfactory. This corroborates that our approach of calculating ionization energies and then adding breadth to the spectra by taking into account the ground-state (zero point) vibrations includes the main factors. Note that the calculated spectrum of the $(H_2O)_6$ prism for the comparison with liquid water additionally contains solvent effects modeled by the polarizable continuum (PCM) approach.

The intensities of the two more strongly bound valence orbitals, relative to the $1b_1$ peak, are compared to literature data in Table 1. For a photon energy of 30 eV and gaseous water, the agreement between different literature data sets is far from

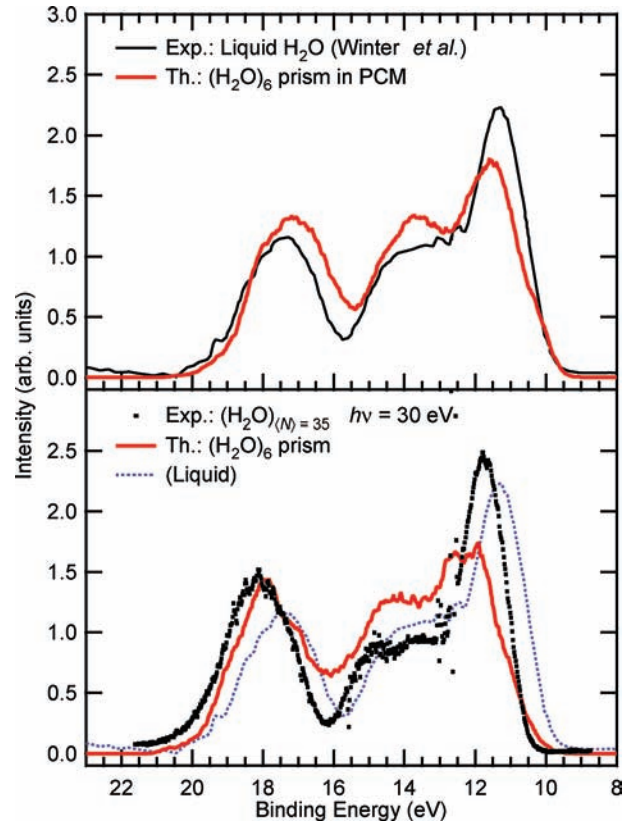

Figure 5. Bottom panel: Outer valence photoelectron spectrum of water clusters, comparison of experiment (symbols: $\langle N \rangle = 35$, $h\nu = 30$ eV) to theory (solid line: $(H_2O)_6$ prism, PMP2/TDDFT approach). Top panel: Outer valence photoelectron spectrum of water, comparison of theory (light solid line: $(H_2O)_6$ prism, PMP2/TDDFT approach, solvent effects taken into account by the PCM model) to experimental liquid water spectrum (dark solid line, from Winter et al.[2]). For reference, the latter spectrum is repeated in the bottom panel as a dotted line.

TABLE 1: Valence Cross Sections of Water Clusters Compared to Values for Gaseous and Liquid Water[a]

	photon energy (eV)	$3a_1$	$1b_2$
cluster, $\langle N \rangle = 30$	30	0.68(8)	0.93(15)
gas	30	0.80(4)	1.26(18)
gas (ref 32)	30	0.71(4)	1.23(5)
gas (ref 31)	30	0.97(3)	1.15(6)
cluster, $\langle N \rangle \approx 8$	61	0.85(10)	0.90(10)
gas	61	0.86(2)	0.77(5)
gas (ref 31)	60	0.89(1)	0.77(1)
gas (ref 2)	60	0.84	0.79
liquid (ref 2)	60	0.69	0.39

[a] Cross sections of the $3a_1$ and $1b_2$ state are given relative to the $1b_1$ line.

perfect, while our gas-phase data are in between. For clusters, intensities are smaller for both orbitals considered here; however, deviations from unity (as assumed in the calculations) are still below 30%. For a photon energy of 60 eV, the agreement between all gas-phase data is satisfactory, and differences of the cluster cross sections to the molecular ones are hardly significant. In a recent study on Ar, some of the authors found intracluster inelastic scattering to be the only source of deviations between gas-phase and cluster photoionization cross sections.[47] With respect to the liquid data, we note that these were derived from measurements at $\theta = 90°$ relative to the photon polarization direction, and cross sections were calculated using angular distribution parameters from the monomer. The good agreement of our calculations to the measured data (top panel in Figure 5)

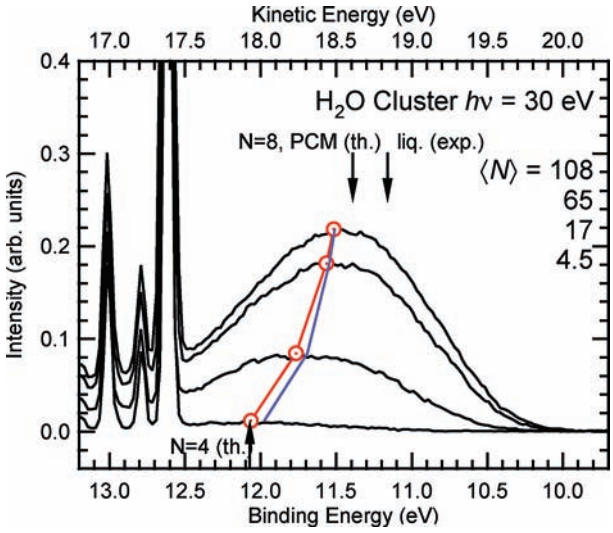

Figure 6. Photoelectron spectra of a water cluster jet with different values of the cluster mean size $\langle N \rangle$, namely, 4.5, 17, 65, and 108 from bottom to top. Spectra were normalized to equal height of the $v' = 0$ monomer peak. With increasing size, the degree of condensation increases; thus, the cluster feature increases in intensity. Maxima of the cluster HOMO line are marked with a symbol and connected to guide the eye. Similar line positions are found from least-squares fits with Gaussian profiles (line without symbols). Arrows pointing downward: Theoretical binding energy for $(H_2O)_8$ with liquid surroundings (PMP2/TDDFT/PCM approach, see text for details) and the experimental value for liquid water.[2] Arrow pointing upward: Theoretical binding energy for $(H_2O)_4$ (PMP2/TDDFT).

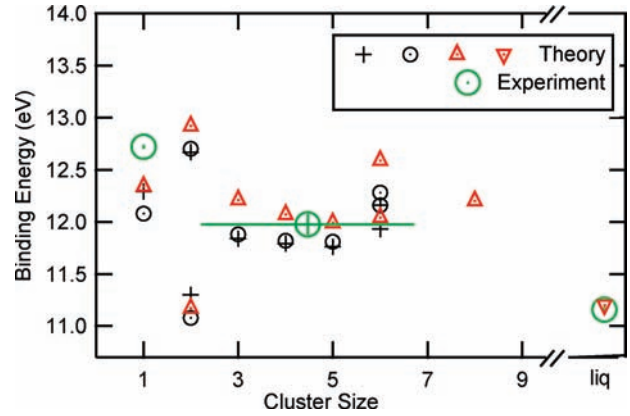

Figure 7. Size dependence of the vertical ionization energy of water clusters: Comparison of different calculational methods with each other, with experiment, and with the limiting values for gas-phase[1] and liquid water.[2] Small symbols: Calculated values (+: CASPT2), (circles: EOM-IP), (triangle: PMP2/TDDFT) (downward pointing triangle: PMP2/TDDFT/PCM). Large symbols: Measured values. The horizontal error bar of the cluster experimental value reflects the approximate width of the cluster size distribution. For the water dimer, inequivalence between the hydrogen donor and the acceptor molecule leads to two different values for the ionization potential (see text for details). For the water hexamer $(H_2O)_6$, two isomers are included.

suggests that, in fact, the β parameters are more isotropic for the liquid. This can easily be understood as an effect of elastic scattering and has been seen, for example, in photoionization studies of Xe clusters.[48]

A splitting of the $3a_1$ peak has been discussed in earlier work on water (e.g., ref 2). It has been argued that this peak splits into two components due to its contribution to hydrogen bonding. Spectroscopic evidence for this is convincingly seen in high-photon-energy (530 eV) photoelectron spectra of ice.[15] In our spectra as well as in photoelectron spectra (PES) of liquid water at lower photon energy, the $3a_1$ state is certainly broadened. However, whether this broadening results from two underlying Gaussians, which overlap to an extent that they can no longer be distinguished, is a matter of interpretation. Our calculations reproduce the peak width well but do not support the existence of two separate components. As the amount of splitting is configuration-dependent,[15] this might be due to averaging over different bonding motifs.

Size Dependence of Water Cluster Ionization Energies. To study the evolution of these features from small clusters toward the infinitely extended liquid, we have recorded a series of spectra of the least strongly bound orbital in which the cluster mean size was varied by changing the expansion temperature (Figure 6). As expected, the binding energy decreases with cluster size and slowly (with $\langle N \rangle^{-1/3}$) converges to the liquid asymptotic value. While the convergence of peak positions is slow, the bandwidth even for clusters of only a few molecules has nearly the same value as that in the liquid. We will now investigate the evolution of peak positions for smaller clusters in some detail and will discuss the convergence toward the liquid limit after that.

For the smallest cluster sizes, we have extracted vertical ionization potentials from our calculations by fitting linear combinations of Gaussian profiles to the calculated spectra, of which one example is shown in Figure 5. The peak maxima found are compared for different calculational methods and different sizes in Figure 7. Full parameters of the Gaussian fits (i.e., positions, widths, and relative intensities of the $1b_1$, $3a_1$, and $1b_2$ peaks) are collected in the Supporting Information. We conclude that the three very different approaches (PMP2/TDDFT, CASPT2, and EOM-IP methods) are mutually consistent, with differences of less than 0.3 eV in peak positions. Qualitatively, the same conclusions hold for relative intensities and full widths at half of the maxima. The agreement between theoretical predictions and the experiment for the water monomer is reasonable both for the PMP2/TDDFT and CASPT2 methods. The ionization energies calculated with the computationally most demanding EOM-IP method surprisingly deviate most from the experimental value for a water monomer, while for larger clusters, parameters from different methods essentially coincide. This can probably be attributed to the influence of the basis set, as shown in ref 19. Therefore, for larger clusters, we have modeled the ionization spectra using the most efficient PMP2/TDDFT scheme.

Similarly to isolated molecular water, also the water dimer represents a special case. The first two ionization potentials (corresponding to ionization from the same orbital) are separated in the equilibrium geometry by about 1.5 eV.[17] This split is a consequence of the nonequivalence of the two water molecules, one acting as a donor and the second as an acceptor of the hydrogen bond. The hydrogen-bond-donor molecule after ionization is significantly stabilized by interaction with the acceptor molecule. Its ionization potential is therefore lowered with respect to the isolated water molecule. For the same reason, the ionization potential corresponding to electron emission from the hydrogen-bond-acceptor molecule is found to increase. In larger water clusters, each molecule plays both roles of donor and acceptor, and no stabilization of particular ionized states occurs, as seen by the delocalization of the molecular orbitals of the water tetramer $(H_2O)_4$ seen in Figure 1.

The comparison of calculated peak maxima to experiment is somewhat hampered by the fact that a jet of clusters produced in a supersonic expansion inevitably contains a distribution of

TABLE 2: Average Mulliken Charges q_1 and q_2 on the Two Most Strongly Charged Water Molecules for the First Ionized State of $(H_2O)_n$ Clusters, Calculated at the TDDFT/BHandHLYP/6-31++g Level and Averaged over 1000 ($n = 2-4$) and 600 ($n = 5, 6, 8$) Geometries, Respectively**

molecule	q_1	q_2
$(H_2O)_2$	0.931	0.069
$(H_2O)_3$	0.695	0.226
$(H_2O)_4$	0.695	0.187
$(H_2O)_5$	0.623	0.206
$(H_2O)_6$, cage	0.676	0.178
$(H_2O)_6$, prism	0.701	0.209
$(H_2O)_8$	0.709	0.143

cluster sizes. Allowing for that, the agreement of our experimental value with the calculations is very good. A complementary assessment of the quality of our calculations can be carried out by comparing them to measured appearance energies, which have recently been collected in a systematic fashion in ref 11. Compared to the vertical ionization energies, cluster-size-resolved values of the appearance energies are measured relatively straightforward by recording partial ion yield spectra versus photon energy.[11] The measured appearance energies for the $(H_2O)_n$, $n = 3-80$, series converge to a value of 10.6 ± 0.2 eV.[11] That is, thus far, the bulk limit of 9.9 eV[2] is not reached. From a theoretical point of view, the appearance energy is a quantity which simultaneously tests the quality of the calculated peak positions and the peak widths. Our calculations agree quantitatively with the experimental values of the appearance energies, with the exception of the values for the water monomer and dimer. Interestingly, for solvated water clusters, the bulk experimental value of 9.9 eV is reached already in the calculation for the $(H_2O)_3$ configuration. For more details, see the Supporting Information.

Two factors can be isolated, which together are causing the trend toward lower ionization potentials with increasing cluster size that is seen in both our measurements and calculations. These are charge delocalization between neighboring water molecules[17] and long-range polarization.[14] The former describes the trend of the final-state charge to become distributed over several molecules, if these form an extended system. In our calculations, we have quantified this final-state property by doing a Mulliken charge analysis, averaged over a number of cluster geometries. As an example of the results in Table 2, we collect the average charge on the two most positive molecules within a cluster of size N. While 93% of the positive charge lays on the donor molecule in the exceptional water dimer case, the charge distribution for $(H_2O)_n$, $n = 3-6$, 8, shows a charge of 0.68 ± 0.04 $|e|$ on the most strongly charged water molecule, with no apparent trend for an increasing size of the system. This situation differs markedly from the charge distribution determined for cluster ions in the local minimum geometry. For example, for the first ionization transition in the $(H_2O)_4$ cluster, all water molecules participate almost equally in the ionization process.[17] However, localization of the charge appears when the molecule moves away from the symmetric local minimum configuration (Table 2).

We now turn to a discussion of larger cluster sizes, for which, from this study, only experimental values are available. In Figure 8, we show the shift of the cluster HOMO binding energy relative to the water monomer as a function of inverse cluster radius, which is proportional to $N^{-1/3}$. It was argued earlier that the cluster size dependence of binding energies in large, nonconducting clusters can be explained by regarding them as a continuous dielectric sphere which is polarized by introduction

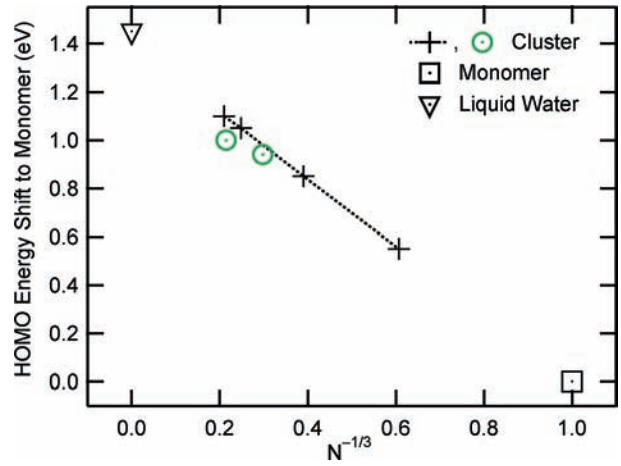

Figure 8. Vertical ionization energies of water clusters relative to the adiabatic ionization energy of molecular water. Crosses: Size-dependent data from Figure 6 (shift of the peak maxima; symbols have been connected to guide the eye). Open circles: Other data (see text). Error bars are about the symbol size. The value for liquid water is from ref 2.

of a positive charge.[49,50] Work is needed to polarize the dielectric substance surrounding the charge, and because of that, lower binding energies are found for larger cluster sizes. The asymptotic value for the infinite liquid is the Gibbs energy of solvation ΔG, which can be calculated by the Born equation for a single vacancy[2,51]

$$\Delta G = -\frac{e^2}{8\pi\varepsilon_0}\left(1 - \frac{1}{\varepsilon}\right)\frac{1}{R} \qquad (1)$$

Here, R is the size of the cavity surrounding the vacancy. For ε, in this application of the Born equation, the permittivity of water at optical frequencies should be used as only contributions from polarization of the electron charge cloud are relevant for the screening in photoionization. It has been shown by Winter et al.[2] that this equation reproduces the energy shift of the liquid (1.45 eV) when an effective cavity radius of $R = 2.24$ Å, suggested in simulations,[52] and a permittivity of $\varepsilon = n^2 = 1.8$ (n: refractive index[53]) are used. For finite clusters, eq 1 has to be modified by replacing the last factor R^{-1} with $(R^{-1} - R_{cl}^{-1})$, where R_{cl} represents the cluster radius as approximated by continuum theory.[50] From that, we see that continuum theory applied to our clusters leads to a straight line in Figure 8, which connects the asymptotic data points for the monomer and the liquid. Within the limits of accuracy of the present experiment, the data shown in Figure 6 follow this behavior. The two additional data points, derived from the overview spectrum in Figure 4 and the data series used for the H_2O, D_2O comparison, reasonably agree with this trend as well. Equation 1, modified to finite cluster size, is rigorously valid only for a vacancy in the exact center of the (assumed spherical) cluster, while for all other sites, slightly lower energy shifts follow.[50] This might be part of the explanation for the deviation of the two latter data points.

The linear relationship between ionization energy and inverse cluster radius observed in Figure 8 and reproduced by eq 1 suggests that this equation can be inverted to provide an empirical measure of the cluster size in an ionization experiment

$$N = \left(\frac{\Delta G}{\Delta G - E_{\mathrm{mono}} + E_{\mathrm{b}}}\right)^3 \quad (2)$$

Here, E_{mono} and E_{b} denote the binding energy of the monomer adiabatic peak (12.615 eV) and the observed binding energy of the cluster signal, respectively. For best agreement with our results, a value for ΔG of 1.4 eV should be used, which is 50 meV lower than the value observed for a liquid jet.[2] Of course, due to the cubic dependence on the energy difference, eq 2 is not of very high accuracy. As an application example, we have calculated the cluster size in the experiment used to determine the outer valence relative ionization cross sections (Table 1). For an energy difference $E_{\mathrm{mono}} - E_{\mathrm{b}}$ of 0.66, we arrive at a mean cluster size of approximately 7, with an error of ±25% from the uncertainty of the experimental energy determination, notwithstanding any systematical shortcomings of our model.

Comparison with D_2O. To assess the importance of zero-point fluctuations, and more generally of cluster geometry effects, on the ionization spectra, it is interesting to compare the water spectra to the ones of deuterated water. We have recorded such spectra as described in the Experimental Section. Visually, spectra of both isotopes at equal photon energy are very similar, apart from the well-known differences in the vibrational frequencies of the monomer.[1] When both sets of spectra are subjected to a least-squares analysis, vertical ionization energies of the normal and deuterated water clusters of 11.69 and 11.74 eV are found. The binding energy difference which follows is 52(4) meV. This difference cannot be explained by the small difference in mean size $\langle N \rangle$ of the clusters, which by linear interpolation of Figure 8 would give a shift of 18 meV in the other direction. Nominal binding energies for both sets of spectra were corrected to reproduce the values of the monomer adiabatic peak[1] (H_2O: 12.615 eV; D_2O: 12.633 eV). The experimental error includes the variance from the measured data sets only, but no assessment of inaccuracies of the underlying reference data is made. Binding energies calculated within the PMP2/TDDFT approach for the tetramer and the prism-shaped hexamer of deuterated water give larger absolute values of the binding energy for clusters from deuterated water, which reproduces the trend shown in the experiment. This once again corroborates that our theoretical method of quantum sampling is well-suited to describe the influence of cluster geometry on the ionization spectra. Full numerical details are given in the Supporting Information.

Discussion

Here, we will relate our findings to a number of other results of cluster photoionization and cluster structure research.

The lack of apparent structure in the cluster photoelectron lines shown in Figure 3 is in contrast to results from photoelectron spectroscopy on noble gas clusters. For those systems, frequently, a surface-to-bulk splitting in photolines from all but the outermost valence orbitals is observed.[49,50,54,55] In at least one instance, even three different inequivalent sites (bulk atoms and surface atoms with two different coordination numbers) were distinguished spectroscopically.[56] A generally accepted explanation of these effects is the difference in polarization screening, which results from the site-dependent differences in the coordination of the ionized atom. Typical surface-to-bulk shifts are values like 185 (Ne 2s) or 300 meV (Ar 3s).[54,55] In water clusters, these values seem to be exceeded by the line broadening due to geometric initial-state effects (see above) and final-state effects from ionization on different points of the cluster ion potential curve.

The broadening of the core-level photoelectron spectrum of water clusters has recently been investigated experimentally and theoretically.[5,57,58] The core-level spectra are as unstructured as our valence HOMO spectra. Phenomenologically, these authors find monomer-to-cluster shifts of approximately 1.3 eV for $\langle N \rangle = 12$ and 1.6 eV for $\langle N \rangle = 45$ cluster. These values are about 0.5−0.6 eV larger than our valence PES shifts. The measured core-level shift for liquid water is also larger than the value for valence orbitals, namely, 1.8 eV.[59] The difference between core- and valence-level shifts might be from the contribution of band structure (initial-state) effects, which can contribute to the observed valence ionization energies, while the initial state in core-level photoionization is simple.[50] A theoretical model has been presented in refs 57 and 58 to explain the shift and the shape of the observed PES by calculating core-level binding energies for typical coordination configurations of a water molecule. Spectra were then simulated by assembling these values according to geometrical information retrieved from molecular dynamics simulation. The results confirmed the measured spectra in general and, in particular, the absence of an observable bulk-to-surface splitting in water clusters. Core-level binding energy differences of different structural motifs were also investigated for liquid water.[59] In this work, calculations of binding energy differences on the Hartree−Fock level were used to interpret depth-specific photoionization experiments using X-rays of variable energy. Both of these works[58,59] find a rather smooth variation of binding energy, with double-donor configurations on the least strongly and single-donor configurations on the more strongly bound side.

Simulated structures of larger water clusters ($N = 20-1000$) were also compared to experiments using IR spectroscopy of the OH stretching vibrations.[60] For clusters with sizes larger than $\langle N \rangle < 200$, two components corresponding to surface and subsurface molecules can be distinguished in the vibrational spectrum, and for sizes larger than $\langle N \rangle < 1000$, a third component corresponding to the crystalline core can be resolved. One could argue that the clusters probed in this work are too small to reflect any of these site dependencies in the photoelectron spectrum; however, water clusters estimated to be much larger (refs 4 and 5) failed to show any site-dependent structure of the valence photoelectron spectrum either.

Summary and Conclusion

Summarizing we have presented a comprehensive study of valence photoionization of water clusters. The line shapes mainly result from orbital energy differences for different cluster geometries. They were successfully modeled by electronic structure calculations supplemented by taking into account a quantum distribution of initial state geometries. The line positions are influenced by final state effects (charge delocalization) for the smaller and long range polarization for the larger clusters. Above about $\langle N \rangle = 8$, binding energies were found to decrease linearly as a function of inverse cluster radius. We suggest that this empirically found relationship (Figure 8) can be used to estimate the mean size of cluster ensembles, for which a scaling law[28] is not applicable, e.g. for a seeded cluster jet, or as a consistency check of the scaling law results.

Acknowledgment. Thanks are due to the BESSY staff for supporting the experimental part of this work. This study was partially funded by the Deutsche Forschungsgemeinschaft and the Fonds der Chemischen Industrie. P.S. would like to acknowledge support of the Ministry of Education of the Czech Republic (Research Project No. 6046137307 and the Czech−

American Cooperation Grant ME08086). M.O. is a student of the International Max Planck Research School "Dynamical Processes in Atoms, Molecules and Solids".

Supporting Information Available: We give the parameters relevant for cluster formation in the described experiments. The cluster size determination via a scaling law is reviewed and discussed. For all calculational schemes and all cluster sizes, the ionization energies and bandwidths for the three outer valence orbitals are given. This material is available free of charge via the Internet at http://pubs.acs.org.

References and Notes

(1) Karlsson, L.; Mattsson, L.; Jadmy, R.; Albridge, R. G.; Pinchas, S.; Bergmark, T.; Siegbahn, K. *J. Chem. Phys.* **1975**, *62*, 4745–4752.

(2) Winter, B.; Weber, R.; Widdra, W.; Dittmar, M.; Faubel, M.; Hertel, I. *J. Phys. Chem. A* **2004**, *108*, 2625–2632.

(3) Tomoda, S.; Achiba, Y.; Kimura, K. *Chem. Phys. Lett.* **1982**, *87*, 197–200.

(4) Björneholm, O.; Federmann, F.; Kakar, S.; Möller, T. *J. Chem. Phys.* **1999**, *111*, 546–550.

(5) Öhrwall, G.; et al. *J. Chem. Phys.* **2005**, *123*, 054310.

(6) Ng, C. Y.; Trevor, D. J.; Tiedemann, P. W.; Ceyer, S. T.; Kronebusch, P. L.; Mahan, B. H.; Lee, Y. T. *J. Chem. Phys.* **1977**, *67*, 4235–4237.

(7) Shiromaru, H.; Shinohara, H.; Washida, N.; Yoo, H.-S.; Kimura, K. *Chem. Phys. Lett.* **1987**, *141*, 7–11.

(8) Stace, A. J. *Phys. Rev. Lett.* **1988**, *61*, 306–309.

(9) de Visser, S. P.; de Koning, L. J.; Nibbering, N. M. M. *J. Phys. Chem.* **1995**, *99*, 15444–15447.

(10) Jongma, R.; Huang, Y.; Shi, S.; Wodtke, A. *J. Phys. Chem. A* **1998**, *102*, 8847–8854.

(11) (a) Belau, L.; Wilson, K. R.; Leone, S. R.; Ahmed, M. *J. Phys. Chem. A* **2007**, *111*, 10075–10083. (b) Addition and Correction: Belau, L.; Wilson, K. R.; Leone, S. R.; Ahmed, M. *J. Phys. Chem. A* **2007**, *111*, 10885–10886.

(12) Ehara, M.; Ishida, M.; Nakatsuji, H. *J. Chem. Phys.* **2001**, *114*, 8990–8999.

(13) Hunt, P.; Sprik, M.; Vuilleumier, R. *Chem. Phys. Lett.* **2003**, *376*, 68–74.

(14) Cabral do Couto, P.; Estacio, S. G.; Cabral, B. J. C. *J. Chem. Phys.* **2005**, *123*, 054510−10.

(15) Nordlund, D.; Odelius, M.; Bluhm, H.; Ogasawara, H.; Pettersson, L.; Nilsson, A. *Chem. Phys. Lett.* **2008**, *460*, 86–92.

(16) Nilsson, A.; Ogasawara, H.; Cavalleri, M.; Nordlund, D.; Nyberg, M.; Wernet, P.; Pettersson, L. G. M. *J. Chem. Phys.* **2005**, *122*, 154505.

(17) Müller, I. B.; Cederbaum, L. S. *J. Chem. Phys.* **2006**, *125*, 204305.

(18) Sodupe, M.; Bertran, J.; Rodriguez-Santiago, L.; Baerends, E. J. *J. Phys. Chem. A* **1999**, *103*, 166–170.

(19) Pieniazek, P. A.; VandeVondele, J.; Jungwirth, P.; Krylov, A. I.; Bradforth, S. E. *J. Phys. Chem. A* **2008**, *112*, 6159–6170.

(20) Kumar, A.; Kołaski, M.; Lee, H. M.; Kim, K. S. *J. Phys. Chem. A* **2008**, *112*, 5502–5508.

(21) Knak Jensen, S. J.; Csizmadia, I. G. *J. Mol. Struct.: THEOCHEM* **1999**, *488*, 263–267.

(22) Tachikawa, H. *J. Phys. Chem. A* **2004**, *108*, 7853–7862.

(23) Furuhama, A.; Dupuis, M.; Hirao, K. *J. Chem. Phys.* **2006**, *124*, 164310–10.

(24) Novakovskaya, Y. V. *Russ. J. Phys. Chem. A* **2007**, *81*, 216–224.

(25) Novakovskaya, Y. V. *Int. J. Quantum Chem.* **2007**, *107*, 2763–2780.

(26) Bobbert, C.; Schulz, C. P. *Eur. Phys. J. D* **2001**, *16*, 95–97.

(27) Barth, S. *Untersuchung des Interatomaren Coulomb-Zerfalls in schwach gebundenen Systemen*. Ph.D. Thesis, Technical University Berlin, Germany, 2007.

(28) Bobbert, C.; Schütte, S.; Steinbach, C.; Buck, U. *Eur. Phys. J. D* **2002**, *19*, 183–192.

(29) Marburger, S. P.; Kugeler, O.; Hergenhahn, U. A molecular beam source for electron spectroscopy of clusters. In *Synchrotron Radiation Instrumentation*, Eighth International Conference; Warwick, T., Arthur, J., Padmore, H. A., Stöhr, J., Eds.; American Institute of Physics: San Francisco, CA, 2003; Vol. 705; pp 1114−1116.

(30) Follath, R.; Schmidt, J. S. A grazing incidence monochromator for the energy range 5−250 eV. In *Synchrotron Radiation Instrumentation*, Eighth International Conference; Warwick, T., Arthur, J., Padmore, H. A., Stöhr, J., Eds.; American Institute of Physics: San Francisco, CA, 2003; Vol. 705, pp 631−634.

(31) Banna, M. S.; McQuaide, B. H.; Malutzki, R.; Schmidt, V. *J. Chem. Phys.* **1986**, *84*, 4739–4744.

(32) Truesdale, C. M.; Southworth, S.; Kobrin, P. H.; Lindle, D. W.; Thornton, G.; Shirley, D. A. *J. Chem. Phys.* **1982**, *76*, 860–865.

(33) Schlegel, H. B. *J. Chem. Phys.* **1986**, *84*, 4530–4534.

(34) Poterya, V.; Farnik, M.; Ončák, M.; Slavíček, P. *Phys. Chem. Chem. Phys.* **2008**, *10*, 4835–4842.

(35) Stanton, J. F.; Gauss, J. *J. Chem. Phys.* **1999**, *111*, 8785–8788.

(36) Cossi, M.; Barone, V. *J. Phys. Chem. A* **2000**, *104*, 10614–10622.

(37) Jagoda-Cwiklik, B.; Slavíček, P.; Cwiklik, L.; Nolting, D.; Winter, B.; Jungwirth, P. *J. Phys. Chem. A* **2008**, *112*, 3499–3505.

(38) Magyar, R. J.; Tretiak, S. *J. Chem. Theory Comput.* **2007**, *3*, 976–987.

(39) Gislason, E. A. *J. Chem. Phys.* **1973**, *58*, 3702–3707.

(40) Della Sala, F.; Rousseau, R.; Görling, A.; Marx, D. *Phys. Rev. Lett.* **2004**, *92*, 183401.

(41) Frisch, M. J.; Trucks, G. W.; Schlegel, H. B.; Scuseria, G. E.; Robb, M. A.; Cheeseman, J. R.; Montgomery, J. A., Jr.; Vreven, T.; Kudin, K. N.; Burant, J. C.; Millam, J. M.; Iyengar, S. S.; Tomasi, J.; Barone, V.; Mennucci, B.; Cossi, M.; Scalmani, G.; Rega, N.; Petersson, G. A.; Nakatsuji, H.; Hada, M.; Ehara, M.; Toyota, K.; Fukuda, R.; Hasegawa, J.; Ishida, M.; Nakajima, T.; Honda, Y.; Kitao, O.; Nakai, H.; Klene, M.; Li, X.; Knox, J. E.; Hratchian, H. P.; Cross, J. B.; Bakken, V.; Adamo, C.; Jaramillo, J.; Gomperts, R.; Stratmann, R. E.; Yazyev, O.; Austin, A. J.; Cammi, R.; Pomelli, C.; Ochterski, J. W.; Ayala, P. Y.; Morokuma, K.; Voth, G. A.; Salvador, P.; Dannenberg, J. J.; Zakrzewski, V. G.; Dapprich, S.; Daniels, A. D.; Strain, M. C.; Farkas, O.; Malick, D. K.; Rabuck, A. D.; Raghavachari, K.; Foresman, J. B.; Ortiz, J. V.; Cui, Q.; Baboul, A. G.; Clifford, S.; Cioslowski, J.; Stefanov, B. B.; Liu, G.; Liashenko, A.; Piskorz, P.; Komaromi, I.; Martin, R. L.; Fox, D. J.; Keith, T.; Al-Laham, M. A.; Peng, C. Y.; Nanayakkara, A.; Challacombe, M.; Gill, P. M. W.; Johnson, B.; Chen, W.; Wong, M. W.; Gonzalez, C.; Pople, J. A. *Gaussian 03*, revision C.02; Gaussian, Inc.: Wallingford, CT, 2004.

(42) Werner, H.-J.; et al. *MOLPRO*, version 2006.1, a package of ab initio programs; see http://www.molpro.net (2006).

(43) Stanton, J.; Gauss, J.; Watts, J.; Szalay, P.; Bartlett, R. with contributions from Auer, A. A.; Bernholdt, D. E.; Christiansen, O.; Harding, M. E.; Heckert, M.; Heun, O.; Huber, C.; Jonsson, D.; Jusélius, J.; Lauderdale, W. J.; Metzroth, T.; Michauk, C.; Price, D. R.; Ruud, K.; Schiffmann, F.; Tajti, A.; Varner, M. E.; Vázquez, J. ACES2 and the integral packages MOLECULE (Almlöf, J.; Taylor, P. R.), PROPS (Taylor, P. R.), and ABACUS (Helgaker, T. Aa.; Jensen, H. J.; Jørgensen, P.; Olsen, J.).

(44) Ahlrichs, R.; Bär, M.; Häser, M.; Horn, H.; Kölmel, C. *Chem. Phys. Lett.* **1989**, *162*, 165.

(45) Reutt, J. E.; Wang, L. S.; Lee, Y. T.; Shirley, D. A. *J. Chem. Phys.* **1986**, *85*, 6928–6939.

(46) Truong, S.; Yencha, A.; Juarez, A.; Cavanagh, S.; Bolognesi, P.; King, G. *Chem. Phys.* **2009**, *355*, 183–193, and references therein.

(47) Hergenhahn, U.; Barth, S.; Ulrich, V.; Mucke, M.; Joshi, S.; Lischke, T.; Lindblad, A.; Rander, T.; Öhrwall, G.; Björneholm, O. *Phys. Rev. B* **2009**, *79*, 155448.

(48) Öhrwall, G.; Tchaplyguine, M.; Gisselbrecht, M.; Lundwall, M.; Feifel, R.; Rander, T.; Schulz, J.; Marinho, R. R. T.; Lindgren, A.; Sorensen, S. L.; Svensson, S.; Björneholm, O. *J. Phys. B* **2003**, *36*, 3937–3949.

(49) Björneholm, O.; Federmann, F.; Fössing, F.; Möller, T. *Phys. Rev. Lett.* **1995**, *74*, 3017–3020.

(50) Björneholm, O.; Federmann, F.; Fössing, F.; Möller, T.; Stampfli, P. *J. Chem. Phys.* **1996**, *104*, 1846–1854.

(51) Atkins, P. W. *Physical Chemistry*; Oxford University Press: Oxford, U.K., 1994.

(52) Bader, J. S.; Cortis, C. M.; Berne, B. J. *J. Chem. Phys.* **1997**, *106*, 2372–2387.

(53) *CRC Handbook of Chemistry and Physics*, 76th Edition; Lide, D. R., Ed.; CRC Press: Boca Raton, FL, 1996.

(54) Feifel, R.; Tchaplyguine, M.; Öhrwall, G.; Salonen, M.; Lundwall, M.; Marinho, R. R. T.; Gisselbrecht, M.; Sorensen, S. L.; Naves de Brito, A.; Karlsson, L.; Mårtensson, N.; Svensson, S.; Björneholm, O. *Eur. Phys. J. D* **2004**, *30*, 343–351.

(55) Öhrwall, G.; Tchaplyguine, M.; Lundwall, M.; Feifel, R.; Bergersen, H.; Rander, T.; Lindblad, A.; Schulz, J.; Peredkov, S.; Barth, S.; Marburger, S.; Hergenhahn, U.; Svensson, S.; Björneholm, O. *Phys. Rev. Lett.* **2004**, *93*, 173401.

(56) Hatsui, T.; Setoyama, H.; Kosugi, N.; Wassermann, B.; Bradeanu, I. L.; Rühl, E. *J. Chem. Phys.* **2005**, *123*, 154304.

(57) Abu-samha, M.; Børve, K. J. *J. Chem. Phys.* **2008**, *128*, 154710.

(58) Abu-samha, M.; Børve, K. J.; Winkler, M.; Harnes, J.; Sæthre, L. J.; Lindblad, A.; Bergersen, H.; Öhrwall, G.; Björneholm, O.; Svensson, S. *J. Phys. B* **2009**, *42*, 055201.

(59) Winter, B.; Aziz, E. F.; Hergenhahn, U.; Faubel, M.; Hertel, I. V. *J. Chem. Phys.* **2007**, *126*, 124504.

(60) Buch, V.; Bauerecker, S.; Devlin, J. P.; Buck, U.; Kazimirski, J. K. *Int. Rev. Phys. Chem.* **2004**, *23*, 375–433.

JP906113E